Mid-infrared, optically active black phosphorus thin films on centimeter scale

Naoki Higashitarumizu[1,2], Tetsuya Kawashima[3], Thomas Smart[4], Reed Yalisove[2,5,6], Chun Yuen Ho[1,2,7], Morten Madsen[7], Daryl C. Chrzan[2,5], Mary C. Scott[2,5,6], Raymond Jeanloz[4], Hitoshi Yusa[3], and Ali Javey[1,2]*

[1]Electrical Engineering and Computer Sciences, University of California, Berkeley, CA 94720, USA
[2]Materials Sciences Division, Lawrence Berkeley National Laboratory, Berkeley, CA 94720, USA
[3]Research Center for Materials Nanoarchitectonics, National Institute for Materials Science (NIMS), Tsukuba, Ibaraki 305-0044, Japan
[4]Department of Earth and Planetary Science, University of California, Berkeley, CA 94720, USA
[5]Department of Materials Science and Engineering, University of California, Berkeley, California 94720, United States
[6]National Center for Electron Microscopy, Molecular Foundry, Lawrence Berkeley National Laboratory, Cyclotron Road, Berkeley, California 94720, USA
[7]Centre for Advanced Photovoltaics and Thin-Film Energy Devices (SDU CAPE), Mads Clausen Institute, University of Southern Denmark, 6400 Sønderborg, Denmark

*Address correspondence to: ajavey@berkeley.edu

Keywords: black phosphorus, mid-infrared emission, high-pressure synthesis, large-scale

ABSTRACT

Black phosphorus (BP) is a narrow bandgap (~0.3 eV) semiconductor with a great potential for optoelectronic devices in the mid-infrared wavelength. However, it has been challenging to achieve a high-quality scalable BP thin film. Here we present the successful synthesis of optically active BP films on a centimeter scale. We utilize the pulsed laser deposition of amorphous red phosphorus, another allotrope of phosphorus, followed by a high-pressure treatment at ~8 GPa to induce a phase conversion into BP crystals. The crystalline quality was improved through thermal annealing, resulting in the observation of photoluminescence emission at mid-infrared wavelengths. We demonstrate high-pressure conversion on a centimeter scale with a continuous film with a thickness of ~18 nm using a flat-belt-type high-pressure apparatus. This synthesis procedure presents a promising route to obtain optical-quality BP films, enabling the exploration of integrated optoelectronic device applications such as light-emitting devices and mid-infrared cameras on a chip scale.

Among the allotropes of phosphorus, black phosphorus (BP) emerges as the most stable phase exhibiting a direct bandgap of approximately 0.3 eV in its bulk state.[1,2] At ambient conditions, BP assumes a puckered structure (orthorhombic, *Cmce*) distorted from its cubic state (*Pm*-3*m*).[3] This distinctive crystal structure imparts a strong in-plane anisotropy across electronic, thermoelectric, and optical properties,[1,4] facilitating highly sensitive bandgap modulation through lattice strain[5] and maintaining a low Auger recombination rate.[6] Photonic devices of remarkable performance have been demonstrated with exfoliated BP flakes, showcasing features such as high detectivity ($D^* > 10^{10}$ cm $Hz^{1/2}W^{-1}$) at room temperature (RT);[7–10] widely tunable light sources covering wavelengths from 2.3 to 7.7 μm by applying strain or electric fields;[5,11] and light-emitting diodes (LEDs) with a long operational lifetime (15,000 hours half-life).[12] Despite its considerable promise for next-generation infrared (IR) devices, surpassing existing technologies based on II-VI or III-V semiconductors (e.g., InSb, HgCdTe), the large-scale implementation of BP thin films has faced impediments due to the absence of chip-to-wafer scale thin film growth,[13,14] setting it apart from other van der Waals materials like graphene, *h*-BN, and transition-metal dichalcogenides (MoS_2, WSe_2).[15–19] This limitation arises from less controllable lateral growth, influenced by large surface energies and robust interlayer forces stemming from sp^3 hybridization, featuring a lone-pair in BP's puckered structure.[3,13]

Recently, the synthesis of subcentimeter-sized single-crystal BP films has been achieved through chemical vapor deposition (CVD), where control over the diffusion of growth precursors is paramount.[14] However, a tradeoff persists between thickness and lateral size, making millimeter-wide films challenging for thicknesses below 100 nm,[14] a critical parameter for optimal optoelectronic device performance.[8] In addition to CVD, pulsed laser deposition (PLD) has been employed to produce high-quality few-to-monolayer BP films on a centimeter scale, yet faces challenges with a narrow growth window and degradation of thicker films (>10 nm) during

prolonged growth due to excess heating.[13,20] Both CVD and PLD methods face the fundamental challenge posed by delicate thermal instability and unmanageable vapor pressure of phosphorus.[21]

To overcome these challenges and advance BP device applications to chip-scale size, we present an upscaling of BP film synthesis to centimeter sizes using crystallographic strategies in contrast to intricate chemical routes. Red phosphorus (red-P), another phosphorus allotrope, proves capable of large-scale growth via thermal evaporation and PLD.[20,22,23] Initiated from amorphous red-P, a high-pressure-induced conversion into BP crystal has been demonstrated using diamond anvil cells (DAC) and multi-anvil cells.[22–25] Notably, this high-pressure conversion technique has successfully yielded highly crystalline thin-film BP up to 5 mm in size, exhibiting a field-effect mobility of 160 $cm^2V^{-1}s^{-1}$ at RT.[23] While electrical devices have been explored, optical characterizations such as photoluminescence (PL) remain limited.

In this paper, we present the successful centimeter-scale conversion of red-P to BP using a flat-belt-type high-pressure apparatus. The red-P film was deposited on a mica substrate via PLD, and a hydrostatic pressure of approximately 8 GPa was induced to convert amorphous red-P into BP crystal. The crystalline quality was enhanced through the optimization of in-situ thermal annealing conditions, as confirmed by Raman and mid-IR PL spectroscopies, achieving a uniform ~18 nm thin film on a centimeter scale without microcracks. This technique offers a platform for further exploration of mid-IR applications based on BP, including LEDs and image sensors.

A red-P film was grown on mica substrate (natural muscovite) via PLD, as illustrated in Figure 1a (details in Experimental Section and Figure S1, Supporting Information). Broad Raman peaks span 350–460 cm^{-1} are observed for red-P deposited at 150°C, and these peaks become progressively distinct with increasing growth temperature up to 250°C (Figure S2a,

Supporting Information). The successful growth of red-P thin film (10–30 nm) resulted in a light brown color, as shown in Figure 1b. Beyond 300°C, film formation exhibited unevenness, and Raman peaks were quenched due to severe decomposition at elevated temperatures (Figure S2a,b). This critical temperature aligns with findings from prior PLD growth experiments.[20] Figure 1c presents a comparative analysis of red-P films grown on different substrates: natural muscovite and 50 nm SiO_2/Si. In contrast to the mica substrate, no obvious red-P fingerprint was confirmed for the as-deposited film on SiO_2/Si, possibly owing to differences in surface energy and roughness.[13] The mica surface is cleaved before growth to create a fresh, atomically flat surface conducive to phosphorus atoms, facilitating surface migration. Figure 1d illustrates a pressure–temperature diagram for red-P to BP conversion, encompassing orthorhombic, rhombohedral, cubic, and liquid BP phases.[26] An experimental relationship, derived from previously reported work on bulk BP growth, is presented as a dashed line in Figure 1d.[27] At ambient pressure, a phase transition occurs around 560°C, decreasing linearly with pressure, enabling room temperature conversion at pressures exceeding 8 GPa. Notably, our approach involves a phase transformation at room temperature under a high pressure of 8 GPa, as opposed to a high-temperature process at lower pressure, aiming to prevent unexpected surface degradation critical for thin film growth, in contrast to bulk growth.

As a proof of concept, we performed high-pressure treatment using DAC. A piece of red-P sample grown at 250°C was placed in the DAC with Al_2O_3 powder serving as the pressure medium, as shown in Figure 2a. In situ Raman measurements were performed through a diamond window. Figure 2b illustrates Raman spectra acquired at various pressures. Under compression at 8 GPa, two peaks were observed at approximately 310 and 370 cm^{-1}, consistent with the results of a prior study on the pressure-dependent Raman spectrum of BP.[28] Additionally, the conversion was visually validated by a shift in sample color from light brown

(red-P) to a lustrous metallic shade (BP), indicative of bandgap narrowing (Figure S3, Supporting Information).[29] While the conversion between red-P and BP phases proved reversible upon decompression to ambient pressure after being held at 8 GPa for 3 or 30 minutes, the BP phase persisted at ambient pressure after exposure to high pressure for over 4 hours (Figure 2b). To convert red-P into BP crystal, P–P bonds have to be activated with *spd* hybridization (details in Figure S4, Supporting Information).[27,30] At the ambient pressure, the conversion rate into BP is slow due to a large activation energy: a thermodynamic model estimates that it takes months to convert red-P into BP at 300°C.[30] A high-pressure above 6.6–7.5 GPa accelerates the conversion rate, red-P can be converted into rhombohedral BP at RT in a reasonable time scale (few hours to 3 days in experiments).[22,24,31] Note that, in this work, the crystallization takes place in rhombohedral BP phase at 8 GPa. After releasing the compression, the rhombohedral BP transits into orthorhombic structure (Figure S4, Supporting Information). To explore substrate effects, red-P deposition and high-pressure conversion were conducted on different mica substrates: natural muscovite ($KAl_3Si_3O_{10}(OH)_2$) and synthetic fluorphlogopite ($KMg_3AlSi_3O_{10}F_2$). Both substrates exhibited comparable quality in as-deposited red-P and synthesized BP films, as evidenced by Raman spectroscopy (Figure S5, Supporting Information), although the muscovite sample displayed a smoother surface profile as compared to synthetic fluorphlogopite (Figure S6, Supporting Information). Moreover, muscovite has larger tensile strength and elastic modulus than other mica substrates, such as synthetic fluorphlogopite and natural phlogopite ($KMg_3AlSi_3O_{10}(OH)_2$), preventing microcracks in the substrates due to the shear strain during the high-pressure process. Consequently, the muscovite substrate was utilized in this study, unless otherwise specified. As shown in Figure 2b, the Raman spectrum exhibited BP signatures during decompression from 8 to 0 GPa. Figure 2c shows Raman spectra from synthesized BP via high-pressure process with and without annealing. For comparison, a Raman spectrum from an

exfoliated BP flake is also presented (Figure 2c). The Raman spectrum of the high-pressure converted BP (8 GPa/RT) displayed broader peaks than the BP reference; notably, the A_g^1 peak at 370 cm^{-1} shows a full width at half maximum (FWHM) of 11.3 cm^{-1}, broader than that of the BP reference (FWHM ~ 1.8 cm^{-1}). To improve the BP crystalline quality, in situ annealing was performed following the phase conversion from red-P to BP. The DAC was annealed in the furnace in nitrogen atmosphere at 300°C for 4 hours. The FWHMs were dramatically reduced for A_g^1 and other peaks, B_{2g} and A_g^2 at ~440 and ~470 cm^{-1}, respectively. Figure 2d shows time evolution of FWHM for Raman peaks over 12 hours. Prolonged annealing effectively decreased the FWHM, although it tended to saturate after 4 hours. Specifically, the FWHM of A_g^1 peak was suppressed by 50% after 12 hours annealing. Increasing the annealing temperature to 400°C expedited the decrease in peak width; however, the FWHM saturated at 5.6, 8.6, and 5.6 cm^{-1} for A_g^1, B_{2g}, and A_g^2 peaks, respectively, possibly due to a fundamental limitation in the crystallinity achieved through the present technique (Figure S7, Supporting Information). Above 500°C, the Raman spectrum quenched due to sample degradation resulting from excess annealing.

To scale up the red-P to BP phase conversion, a flat-belt-type high-pressure apparatus was employed (Figure 3a).[32] The PLD red-P film on mica was sandwiched between pyrophyllite and NaCl-ZrO_2 disks, as the pressure medium, enclosed by a graphite heater (Figure 3b, and details in Figure S8, Supporting Information). To prevent potential damage to the red-P/mica sample due to microcracks when embedded directly in the pressure medium, dummy mica substrates were interposed between the sample and pyrophyllite, serving as a buffer layer to mitigate shear stress during compression. The red-P sample was placed exactly at the center of the pressurized area in the vertical direction to minimize the uneven stress. In the DAC experiment, the use of alumina as the pressure medium could cause significant differential stress. In comparison, the synthesis experiment using the flat-belt-type apparatus, which uses a softer

pressure medium (NaCl-ZrO_2), is considered to be more quasi-hydrostatic than the DAC experiment due to the combined effect of the dummy mica placed above and below the sample to mitigate the differential stress generation. By mitigating microcracks, a uniform thin BP film on a centimeter scale was achieved through high-pressure conversion at 7.7 GPa for 5 hours, as shown in the optical images in Figure 3c,d. The film thickness was revealed to be ~18 nm by atomic force microscopy (AFM), as shown in Figure S9, Supporting Information. Together with optical images, an atomically flat surface was confirmed by AFM (Figure 3e). The typical root mean roughness was 0.87 nm. The uniformity was verified at different spots across the centimeter scale BP film (Figure S10, Supporting Information). Due to the scaled-up conversion process, additional material characterization options became available, including X-ray diffraction (XRD). Figure 3f presents a $\theta/2\theta$ XRD scan for the as-deposited red-P film and BP film after the high-pressure process, with and without in situ annealing at 300°C for 5 hours. Similar to the as-deposited red-P film, the BP film without thermal annealing exhibited no peaks other than background peaks from the mica substrate, while the BP film revealed BP peaks following in-situ annealing. To further investigate the crystallinity of synthesized BP film, a plan-view transmission electron microscopy (TEM) was performed on a BP film isolated from the growth substrate (details in Experimental Section). BP films were polycrystalline, with grain size ranging from 40 nm to 200 nm as shown in Figure 3g and Figure S11a–c, Supporting Information. Figure 3g displays a high-resolution plan-view TEM image of a single grain of BP crystal that reveals layered structure. The interlayer distance was found to be 5.5 Å, which mathces well with the reported value of 5.2–5.6Å along [010] direction.[33] Fast-Fourier-transforms (FFT) of the TEM images suggest the presence of an amorphous phosphorus (Figure 3h and Figure S11d, Supporting Information).

Figure 4a shows Raman spectra for synthesized BP film with annealing at 300, 350, and 400°C, for 5 hours. Similar to the results from DAC experiments (Figure S7, Supporting Information), crystalline quality exhibited less dependence on annealing temperature through the scaled-up high-pressure process. As illustrated in Figure 4b, Raman mapping measurements indicated uniform quality of the BP film. Figure 4c presents photoluminescence (PL) spectra from the as-deposited red-P and synthesized BP film (7.7 GPa, 300°C). The ~18 nm thick BP film displayed a mid-IR emission at around 0.3 eV, corresponding to the inherent bandgap of BP. Along with the primary emission from band-to-band transition, a sub-peak was observed at ~0.5 eV, likely attributable to a residual strain after the high-pressure procedure.[5,34,35] As demonstrated in the temperature-dependent PL spectrum, the band-to-band PL emission became sharper and red-shifted at low temperature, consistent with the temperature-dependent PL in exfoliated BP flakes.[5] Notably, this marks the first report on the observation of PL from a BP thin film (10–20 nm) on a centimeter scale. Given that PL emission is more sensitive to defects and impurities than other crystallographic characterizations such as Raman and XRD, these findings should catalyze further investigations into large-scale optoelectronic devices, such as mid-IR LEDs and photodetectors based on high-pressure synthesized BP films.

We have successfully demonstrated the synthesis of optically active large-scale BP thin films through high-pressure, high-temperature conversion from red-P films. Applying high-pressure (~8 GPa) to the amorphous red-P film deposited on a mica substrate using pulsed laser deposition induced a phase conversion into polycrystalline BP. Employing a flat-belt-type high-pressure apparatus, as opposed to diamond anvil cells, allowed for the upscaling of the technique to the centimeter scale, resulting in the production of a uniform, crack-free BP film. The crystalline quality was further enhanced through annealing at 300°C, showcasing photoluminescence emission at mid-infrared wavelengths. This pioneering technique facilitates

the creation of optical-quality BP films, opening avenues for the exploration of chip-scale mid-infrared optoelectronic device applications.

METHODS

Preparation of the red-P film

Amorphous red-P films were grown on target substrates via pulsed laser deposition (PLD) using a KrF laser (λ = 248 nm). A 50 nm SiO_2/Si, natural muscovite ($KAl_3Si_3O_{10}(OH)_2$), and synthetic fluorphlogopite ($KMg_3AlSi_3O_{10}F_2$) were used as the growth substrate, and placed at 70 mm above the PLD target of bulk BP (Smart Elements) that is less reactive than red-P source so the plasma plume is more stable. A Si substrate was attached on the growth substrate to increase the thermal transfer from the lamp heater (Figure 1a). For mica substrates, a fresh surface was cleaved before sample loading. The substrate was preheated at 500°C for 30 min to remove water molecules absorbed on substrate and sample stages. After cooling the substrate to the target temperature at 150–350°C, a red-P film was deposited with a laser energy and pulse frequency of 200 mJ and 10 Hz, respectively. The sample was unloaded to the load lock chamber just after deposition, then nitrogen gas was introduced to cool down the sample. The unloading time was minimized (~40 sec) to reduce excess annealing effects, which is critical for high crystalline quality. For the high-pressure experiments, a ~18 nm red-P film was grown at 250°C and 5 min. To prevent surface modification, red-P samples were sealed in nitrogen and carried for additional processing and characterizations.

High-pressure experiments

A piece of red-P on mica was placed in the DAC with Al_2O_3 powder as a pressure medium. The Al_2O_3 powder was ground in a tungsten carbide mortar and pestle while submerged in acetone until a particle size of ~1 μm was achieved. To calibrate the pressure, a ruby particle was loaded adjacent to the red-P sample. Quasi-hydrostatic pressure of 8–10 GPa was sustained for 5 hours to complete the phase conversion into BP. For the thermal annealing, the DAC was heated at the

target temperature of 300°C, 400°C, and 500°C for 0.5–12 hours after the phase conversion under high pressure at RT. During the annealing, the pressure was kept at 8–10 GPa. After the annealing, the DAC was naturally cooled down to RT. The pressure was gradually released over a 9-hour period in order to change the BP crystal structure from rhombohedral to orthorhombic. To scale up the BP film synthesis, phase conversion was conducted in a flat-belt-type high-pressure apparatus (Figure 3a,b, and Figure S8, Supporting Information). An 8×8 mm^2 red-P/mica sample was pressurized with pyrophyllite and NaCl-ZrO_2 disks. To prevent microcracks due to shear force, dummy mica substrates were introduced between the sample and pyrophyllite disks, as buffer layers. The red-P film was converted to rhombohedral BP at 7.7 GPa, which was calibrated with the phase transition of bismuth.[36] Hydrostatic pressure was applied at different temperatures, RT and 300–400°C. After cooling down to RT, the pressure was released over 90 min to change the BP phase to orthorhombic.

Crystallographic characterization

XRD patterns were obtained using a Rigaku SmartLab X-ray diffractometer (Cu Kα radiation). To prepare the BP on a carbon net for TEM measurements, the BP/mica sample was dipped in 1% HF, isolating the BP film by etching the mica substrate. A carbon net was used to scoop up the BP film floating on HF, following a drying process in vacuum to remove water residue. High-resolution TEM images were acquired on a FEI Titan microscope with a field emission gun operating at accelerating voltage of 300 kV.

Optical characterization

Raman spectra were measured by a PL/Raman microscopic system (Horiba Labram HR Evolution) with a 473-nm excitation laser. In-situ Raman measurement was performed thorough

the DAC at different pressures, which were calibrated using fluorescience peak positions of the ruby particle measured in the same system. A 20× objective lens (5 μm nominal laer diameter) was used for Raman mapping. The BP film was scanned in 5 μm steps across a 100×100 μm^2 area. Mid-IR PL spectra were measured by an FTIR spectrometer (iS50, Thermo Fisher) with a liquid N_2-cooled HgCdTe detector and a 638-nm excitation laser.[2,5] To prevent oxidation, the samples were placed in vacuum during Raman and PL measurements.

Supporting Information

Schematic of PLD setup, Raman spectra of red-P grown at different temperature, Optical images of red-P and BP samples, Schematic of phase conversion mechanism, Raman spectra of BP film on different mica substrates, AFM topography images of red-P and BP films, FWHM of Raman peaks, Schematic image of flat-belt-type high-pressure apparatus, TEM images of BP film.

Acknowledgements

This work was supported by the U.S. Department of Energy, Office of Science, Office of Basic Energy Sciences, Materials Sciences and Engineering Division under contract no. DE-AC02-05Ch11231 (Electronic Materials program). N. H. acknowledges support from the Postdoctoral Fellowships for Research Abroad of Japan Society for the Promotion of Science. The work in Japan was partly supported by JSPS KAKENHI (19H05790) and World Premier International Research Center Initiative (WPI), MEXT, Japan. M.M. acknowledges Danmarks Frie Forskningsfond, DFF FTP, for funding of the project React-PV, No. 8022-00389B.

REFERENCES

(1) Ling, X.; Wang, H.; Huang, S.; Xia, F.; Dresselhaus, M. S. The Renaissance of Black Phosphorus. *Proc. Natl. Acad. Sci. U. S. A.* **2015**, *112* (15), 4523–4530.

(2) Higashitarumizu, N.; Uddin, S. Z.; Weinberg, D.; Azar, N. S.; Reaz Rahman, I. K. M.; Wang, V.; Crozier, K. B.; Rabani, E.; Javey, A. Anomalous Thickness Dependence of Photoluminescence Quantum Yield in Black Phosphorous. *Nat. Nanotechnol.* **2023**, *18* (5), 507–513.

(3) Burdett, J. K.; McLarnan, T. J. A Study of the Arsenic, Black Phosphorus, and Other Structures Derived from Rock Salt by Bond‐breaking Processes. I. Structural Enumeration. *J. Chem. Phys.* **1981**, *75* (12), 5764‐5773.

(4) Xia, F.; Wang, H.; Jia, Y. Rediscovering Black Phosphorus as an Anisotropic Layered Material for Optoelectronics and Electronics. *Nat. Commun.* **2014**, *5*, 4458.

(5) Kim, H.; Uddin, S. Z.; Lien, D.-H.; Yeh, M.; Azar, N. S.; Balendhran, S.; Kim, T.; Gupta, N.; Rho, Y.; Grigoropoulos, C. P.; Crozier, K. B.; Javey, A. Actively Variable-Spectrum Optoelectronics with Black Phosphorus. *Nature* **2021**, *596* (7871), 232–237.

(6) Bhaskar, P.; Achtstein, A. W.; Vermeulen, M. J. W.; Siebbeles, L. D. A. Radiatively Dominated Charge Carrier Recombination in Black Phosphorus. *J. Phys. Chem. C* **2016**, *120* (25), 13836–13842.

(7) Bullock, J.; Amani, M.; Cho, J.; Chen, Y.-Z.; Ahn, G. H.; Adinolfi, V.; Shrestha, V. R.; Gao, Y.; Crozier, K. B.; Chueh, Y.-L.; Javey, A. Polarization-Resolved Black Phosphorus/Molybdenum Disulfide Mid-Wave Infrared Photodiodes with High Detectivity at Room Temperature. *Nat. Photonics* **2018**, *12* (10), 601–607.

(8) Amani, M.; Regan, E.; Bullock, J.; Ahn, G. H.; Javey, A. Mid-Wave Infrared Photoconductors Based on Black Phosphorus-Arsenic Alloys. *ACS Nano* **2017**, *11* (11), 11724–11731.

(9) Rogalski, A. Detectivities of WS_2/HfS_2 Heterojunctions. *Nat. Nanotechnol.* **2022**, *17* (3), 217–219.

(10) Zhong, F.; Wang, H.; Wang, Z.; Wang, Y.; He, T.; Wu, P.; Peng, M.; Wang, H.; Xu, T.; Wang, F.; Wang, P.; Miao, J.; Hu, W. Recent Progress and Challenges on Two-Dimensional Material Photodetectors from the Perspective of Advanced Characterization Technologies. *Nano Res.* **2021**, *14* (6), 1840–1862.

(11) Chen, C.; Lu, X.; Deng, B.; Chen, X.; Guo, Q.; Li, C.; Ma, C.; Yuan, S.; Sung, E.; Watanabe, K.; Taniguchi, T.; Yang, L.; Xia, F. Widely Tunable Mid-Infrared Light Emission in Thin-Film Black Phosphorus. *Sci Adv* **2020**, *6* (7), eaay6134.

(12) Higashitarumizu, N.; Tajima, S.; Kim, J.; Cai, M.; Javey, A. Long Operating Lifetime Mid-Infrared LEDs Based on Black Phosphorus. *Nat. Commun.* **2023**, *14* (1), 4845.

(13) Wu, Z.; Lyu, Y.; Zhang, Y.; Ding, R.; Zheng, B.; Yang, Z.; Lau, S. P.; Chen, X. H.; Hao, J. Large-Scale Growth of Few-Layer Two-Dimensional Black Phosphorus. *Nat. Mater.* **2021**, *20* (9), 1203–1209.

(14) Chen, C.; Yin, Y.; Zhang, R.; Yuan, Q.; Xu, Y.; Zhang, Y.; Chen, J.; Zhang, Y.; Li, C.; Wang, J.; Li, J.; Fei, L.; Yu, Q.; Zhou, Z.; Zhang, H.; Cheng, R.; Dong, Z.; Xu, X.; Pan, A.; Zhang, K.; He, J. Growth of Single-Crystal Black Phosphorus and Its Alloy Films through Sustained Feedstock Release. *Nat. Mater.* **2023**, *22* (6), 717–724.

(15) Kang, K.; Xie, S.; Huang, L.; Han, Y.; Huang, P. Y.; Mak, K. F.; Kim, C.-J.; Muller, D.; Park, J. High-Mobility Three-Atom-Thick Semiconducting Films with Wafer-Scale Homogeneity. *Nature* **2015**, *520* (7549), 656–660.

(16) Fukamachi, S.; Solís-Fernández, P.; Kawahara, K.; Tanaka, D.; Otake, T.; Lin, Y.-C.; Suenaga, K.; Ago, H. Large-Area Synthesis and Transfer of Multilayer Hexagonal Boron Nitride for Enhanced Graphene Device Arrays. *Nature Electronics* **2023**, *6* (2), 126–136.
(17) Shim, J.; Bae, S.-H.; Kong, W.; Lee, D.; Qiao, K.; Nezich, D.; Park, Y. J.; Zhao, R.; Sundaram, S.; Li, X.; Yeon, H.; Choi, C.; Kum, H.; Yue, R.; Zhou, G.; Ou, Y.; Lee, K.; Moodera, J.; Zhao, X.; Ahn, J.-H.; Hinkle, C.; Ougazzaden, A.; Kim, J. Controlled Crack Propagation for Atomic Precision Handling of Wafer-Scale Two-Dimensional Materials. *Science* **2018**, *362* (6415), 665–670.
(18) Zhu, J.; Park, J.-H.; Vitale, S. A.; Ge, W.; Jung, G. S.; Wang, J.; Mohamed, M.; Zhang, T.; Ashok, M.; Xue, M.; Zheng, X.; Wang, Z.; Hansryd, J.; Chandrakasan, A. P.; Kong, J.; Palacios, T. Low-Thermal-Budget Synthesis of Monolayer Molybdenum Disulfide for Silicon Back-End-of-Line Integration on a 200 mm Platform. *Nat. Nanotechnol.* **2023**, *18* (5), 456–463.
(19) Kobayashi, T.; Bando, M.; Kimura, N.; Shimizu, K.; Kadono, K.; Umezu, N.; Miyahara, K.; Hayazaki, S.; Nagai, S.; Mizuguchi, Y.; Murakami, Y.; Hobara, D. Production of a 100-m-Long High-Quality Graphene Transparent Conductive Film by Roll-to-Roll Chemical Vapor Deposition and Transfer Process. *Appl. Phys. Lett.* **2013**, *102* (2), 023112.
(20) Yang, Z.; Hao, J.; Yuan, S.; Lin, S.; Yau, H. M.; Dai, J.; Lau, S. P. Field-Effect Transistors Based on Amorphous Black Phosphorus Ultrathin Films by Pulsed Laser Deposition. *Adv. Mater.* **2015**, *27* (25), 3748–3754.
(21) Kitada, S.; Shimizu, N.; Hossain, M. Z. Safe and Fast Synthesis of Black Phosphorus and Its Purification. *ACS Omega* **2020**, *5* (20), 11389–11393.
(22) Li, X.; Deng, B.; Wang, X.; Chen, S.; Vaisman, M.; Karato, S.-I.; Pan, G.; Lee, M. L.; Cha, J.; Wang, H.; Xia, F. Synthesis of Thin-Film Black Phosphorus on a Flexible Substrate. *2D Mater.* **2015**, *2* (3), 031002.
(23) Li, C.; Wu, Y.; Deng, B.; Xie, Y.; Guo, Q.; Yuan, S.; Chen, X.; Bhuiyan, M.; Wu, Z.; Watanabe, K.; Taniguchi, T.; Wang, H.; Cha, J. J.; Snure, M.; Fei, Y.; Xia, F. Synthesis of Crystalline Black Phosphorus Thin Film on Sapphire. *Adv. Mater.* **2018**, *30* (6), 1703748.
(24) Rissi, E. N.; Soignard, E.; McKiernan, K. A.; Benmore, C. J.; Yarger, J. L. Pressure-Induced Crystallization of Amorphous Red Phosphorus. *Solid State Commun.* **2012**, *152* (5), 390–394.
(25) Endo, S.; Akahama, Y.; Terada, S.-I.; Narita, S.-I. Growth of Large Single Crystals of Black Phosphorus under High Pressure. *Jpn. J. Appl. Phys.* **1982**, *21* (8A), L482.
(26) Solozhenko, V. L.; Turkevich, V. P–T Phase Diagram of Phosphorus Revisited. *J. Phys. Chem. C* **2023**, *127* (12), 6088–6092.
(27) Sorgoto, I.; Guarise, G. B.; Marini, A. Red to Black Phosphorus Transition up to 65 Kbar. *High Temp. --High Pressures* **1970**, *2*, 405–111.
(28) Akahama, Y.; Kobayashi, M.; Kawamura, H. Raman Study of Black Phosphorus up to 13 GPa. *Solid State Commun.* **1997**, *104* (6), 311–315.
(29) Chaves, A.; Azadani, J. G.; Alsalman, H.; da Costa, D. R.; Frisenda, R.; Chaves, A. J.; Song, S. H.; Kim, Y. D.; He, D.; Zhou, J.; Castellanos-Gomez, A.; Peeters, F. M.; Liu, Z.; Hinkle, C. L.; Oh, S.-H.; Ye, P. D.; Koester, S. J.; Lee, Y. H.; Avouris, P.; Wang, X.; Low, T. Bandgap Engineering of Two-Dimensional Semiconductor Materials. *npj 2D Materials and Applications* **2020**, *4* (1), 1–21.
(30) Pauling, L.; Simonetta, M. Bond Orbitals and Bond Energy in Elementary Phosphorus. *J. Chem. Phys.* **1952**, *20* (1), 29–34.

(31) Zaug, J. M.; Soper, A. K.; Clark, S. M. Pressure-Dependent Structures of Amorphous Red Phosphorus and the Origin of the First Sharp Diffraction Peaks. *Nat. Mater.* **2008**, *7* (11), 890–899.
(32) Kawamura, F.; Yusa, H.; Taniguchi, T. Synthesis of Rhenium Nitride Crystals with MoS_2 Structure. *Appl. Phys. Lett.* **2012**, *100* (25), 251910.
(33) Morita, A. Semiconducting Black Phosphorus. *Appl. Phys. A* **1986**, *39* (4), 227–242.
(34) Rodin, A. S.; Carvalho, A.; Castro Neto, A. H. Strain-Induced Gap Modification in Black Phosphorus. *Phys. Rev. Lett.* **2014**, *112* (17), 176801.
(35) Ye, Y.; Dou, X.; Ding, K.; Chen, Y.; Jiang, D.; Yang, F.; Sun, B. Single Photon Emission from Deep-Level Defects in Monolayer WSe_2. *Phys. Rev. B Condens. Matter* **2017**, *95* (24), 245313.
(36) Bean, V. E.; Akimoto, S.; Bell, P. M.; Block, S.; Holzapfel, W. B.; Manghnani, M. H.; Nicol, M. F.; Stishov, S. M. Another Step toward an International Practical Pressure Scale. *Physica* **1986**, *139–140*, 52–54.

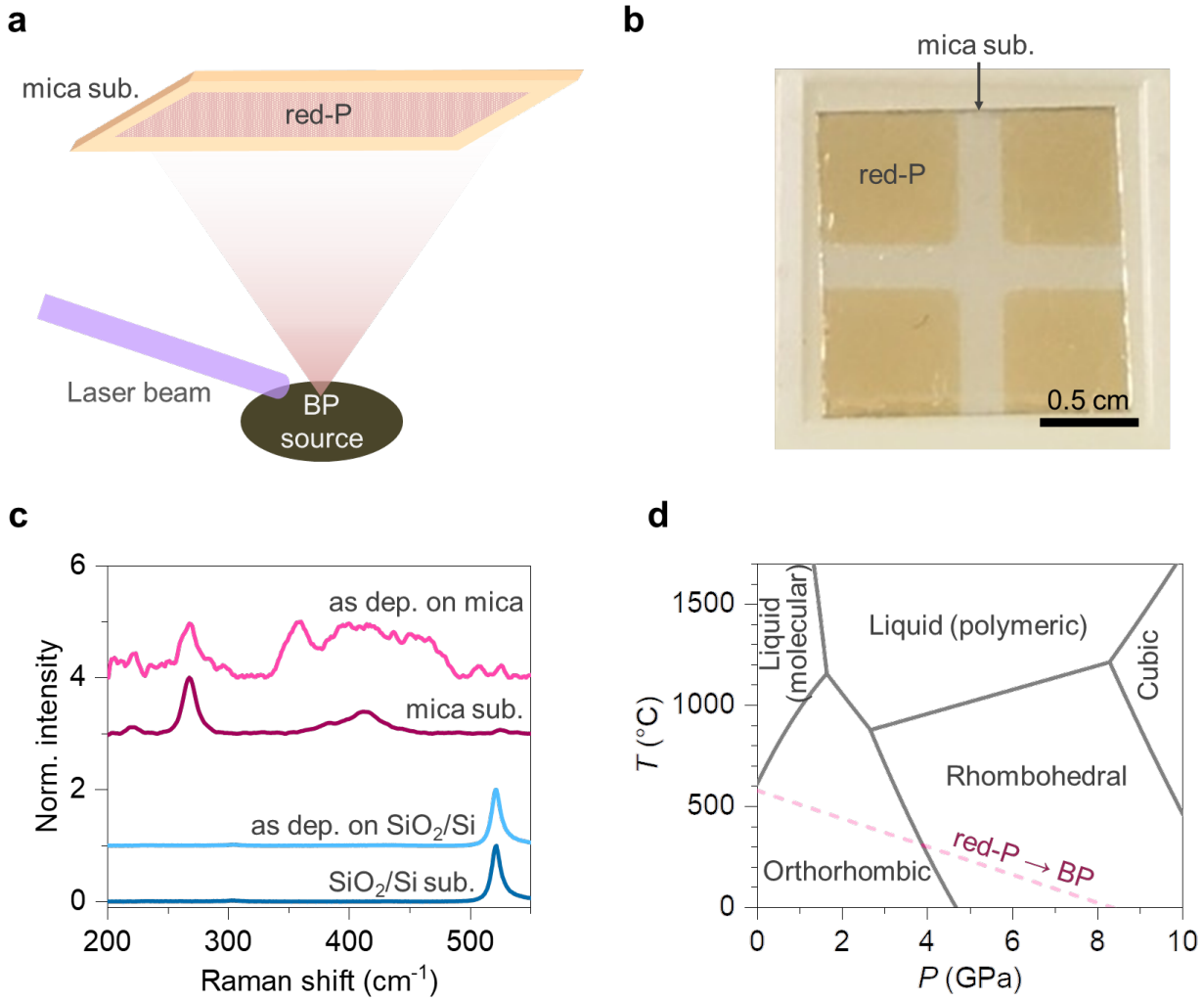

Figure 1. Large scale deposition of red-P and phase conversion to BP. a) Schematic of PLD setup. b) Photographic image of as grown red-P film. c) Raman spectra of as deposited films on SiO_2/Si and mica (natural muscovite) substrate. The film thickness was fixed at 20 nm. d) Phase diagram of BP in different allotropes.[26] Dashed line shows pressure–temperature condition for conversion from red-P to BP.[22,24,27] Reproduced from ref [26]. Copyright 2023 American Chemical Society.

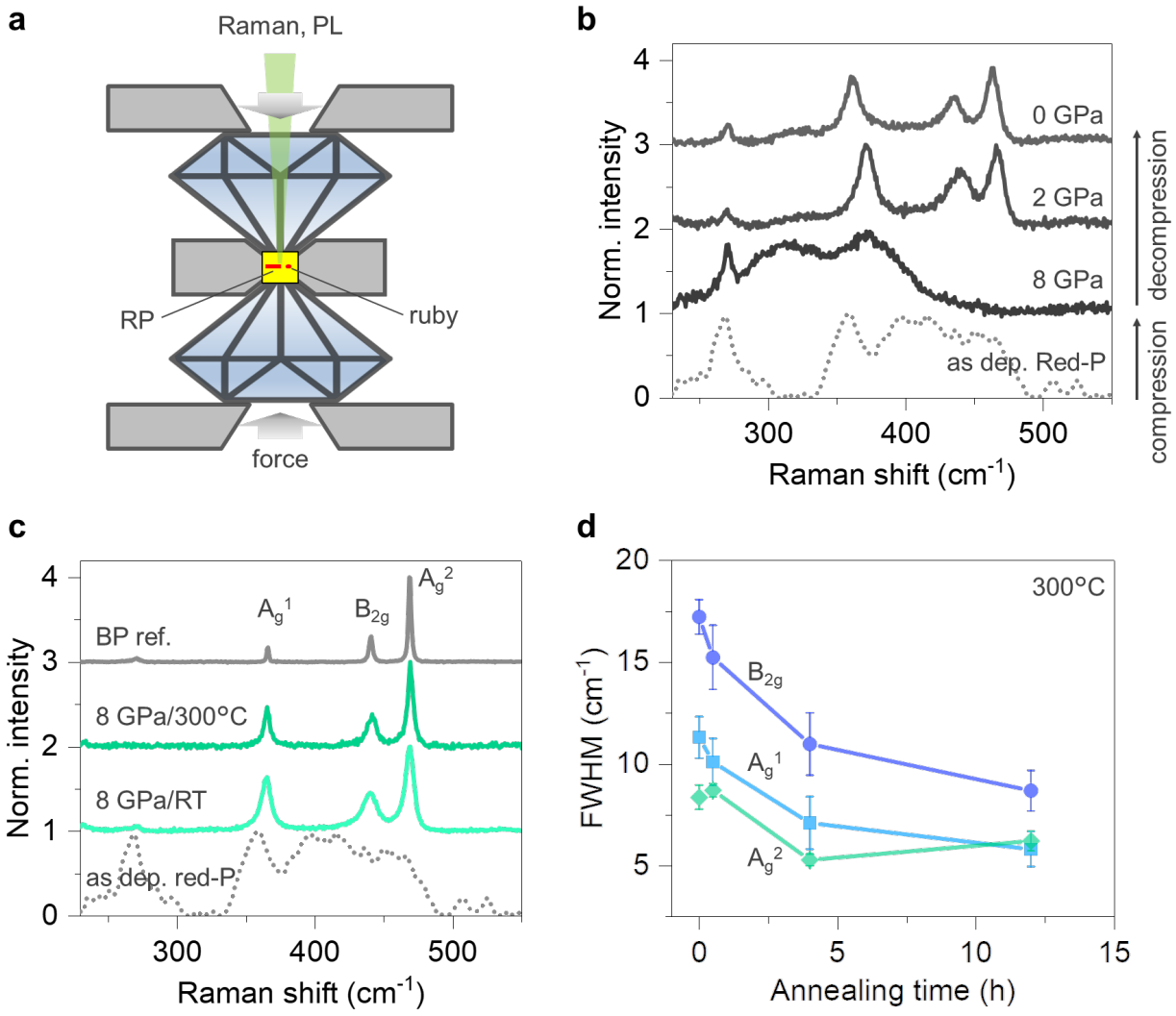

Figure 2. a) Schematic of DAC setup. The red-P film was embedded in Al_2O_3 serving as a pressure medium. A ruby particle was used to measure the applied pressure. b) In situ Raman spectra under different pressure, ~8, ~2, and 0 GPa. The red-P sample was compressed under 8 GPa at RT fist, then the pressure was released to 2 GPa to 0 GPa. c) Raman spectra of the synthesized BP with and without annealing. In situ annealing was performed at 300°C for 4 hours under 8 GPa compression. Raman spectra for as deposited red-P and exfoliated BP flake are also shown as references. d) Effect of annealing time on FWHM for Raman peaks at ~370 cm^{-1} (A_g^1), ~440 cm^{-1} (B_{2g}), and ~470 cm^{-1} (A_g^2). The annealing temperature was fixed at 300°C.

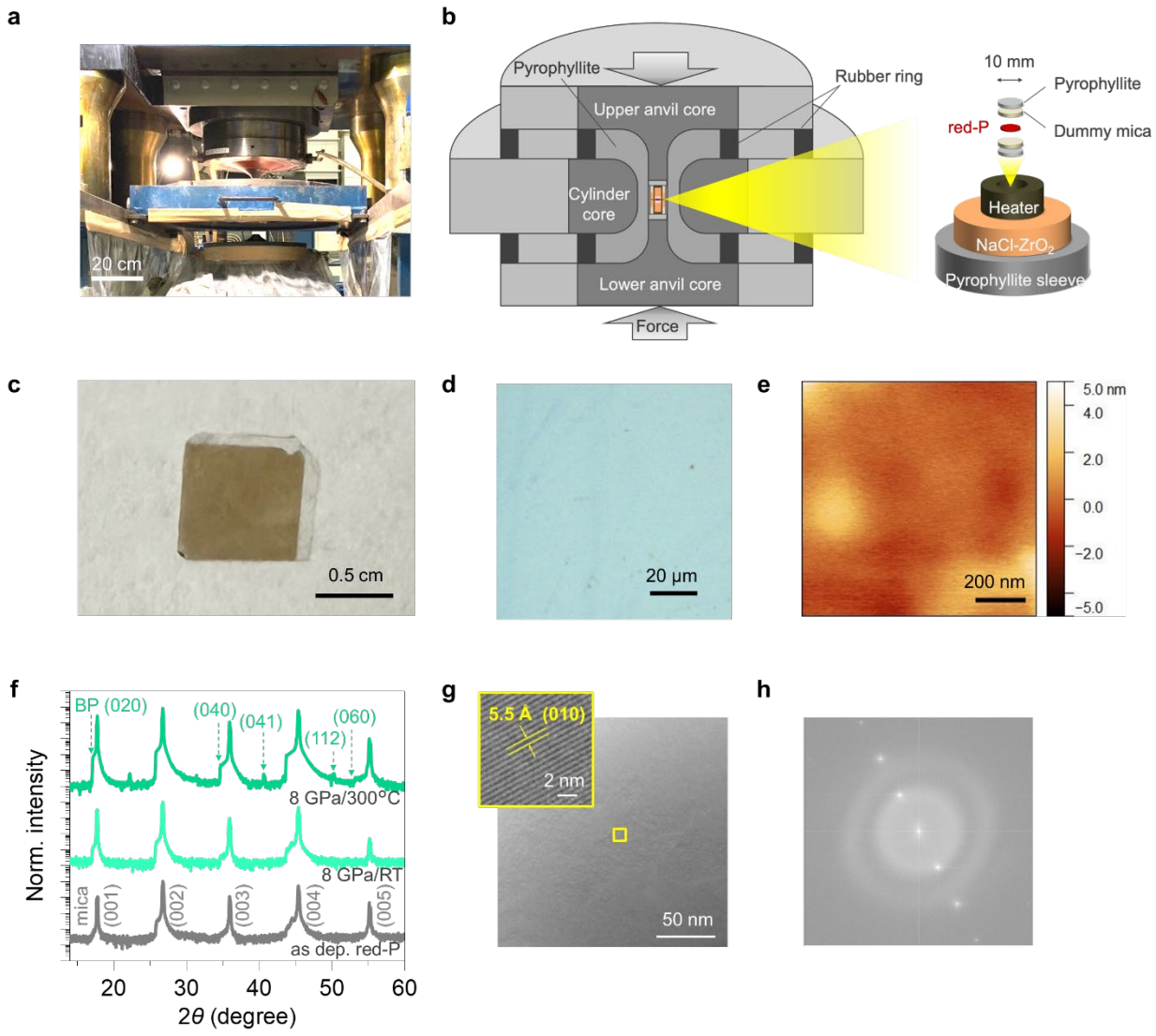

Figure 3. Large scale high-pressure conversion. a) Photographic image of a flat-belt-type high-pressure apparatus. b) Schematic illustration of anvils and a cell assembly for high-pressure experiments. c) Optical images of synthesized BP thin film. The red-P deposited at 250°C was converted into BP under pressure and temperature of 7.7 GPa and 300°C, respectively, for 5 hours. d) Optical microscope image of BP film. e) AFM topographic image on the BP surface. f) XRD patterns of as deposited red-P film; and after high-pressure treatment at RT and 300°C. g,h) High-resolution plan-view TEM image and FFT pattern of BP film.

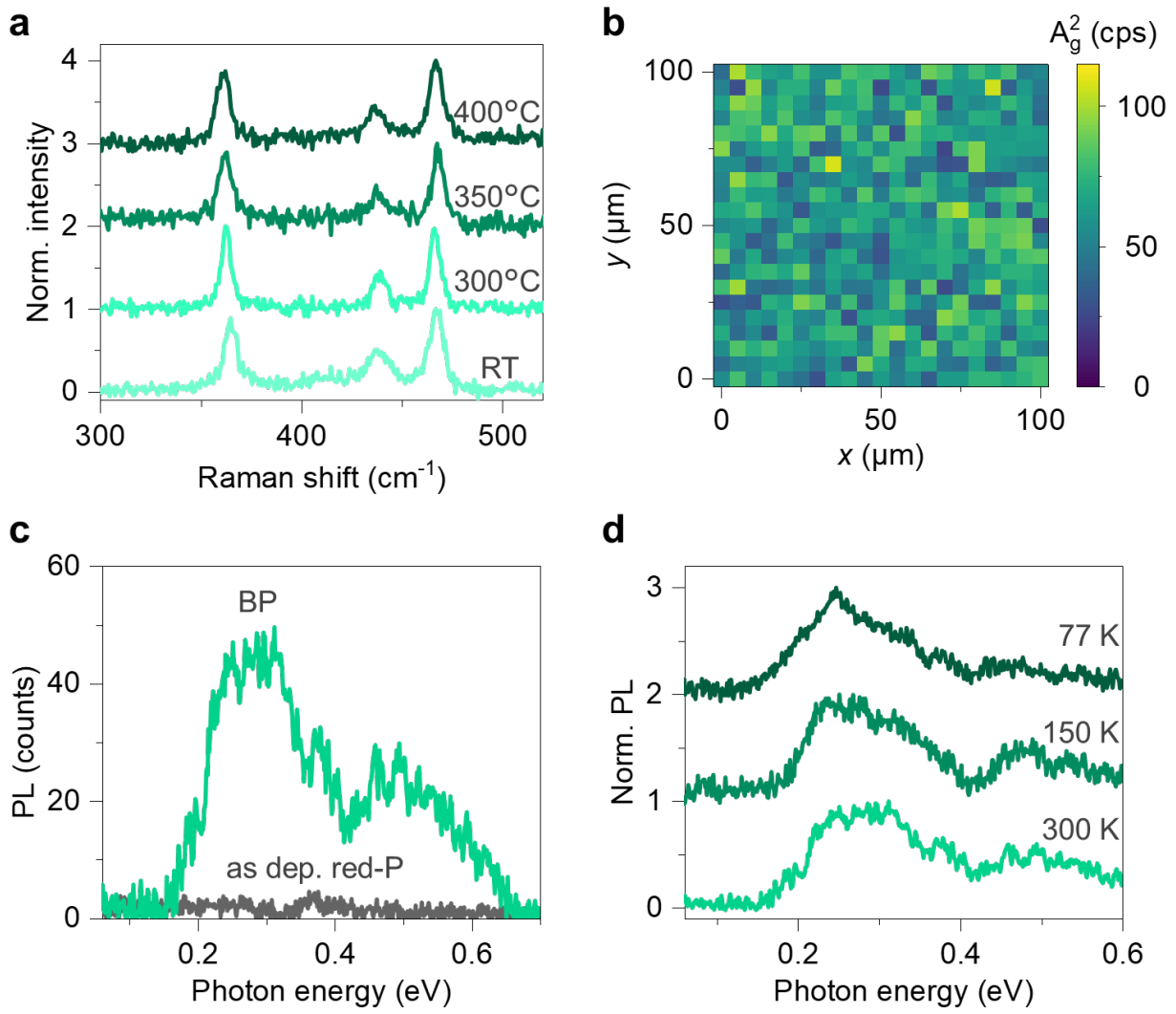

Figure 4. Optical characterizations of high-pressure converted films. a) RT Raman spectra of high-pressure converted BP films at different annealing temperature, 300, 350, 400°C. A BP film after high-pressure treatment under 7.7 GPa at RT serves as a reference. b) RT Raman mapping of BP film annealed at 300°C. c) RT PL spectra of as deposited red-P (250°C) and synthesized BP film (7.7 GPa, 300°C). d) Temperature dependent PL spectrum from synthesized BP film.

Author Contributions

N.H. and A.J. conceived the idea for the project and designed the experiments. N.H. performed red-P deposition via PLD. N.H., T.S. and R.J. performed high-pressure treatment with DACs. T.K. and H.Y. performed high-pressure process with a flat-belt-type high-pressure apparatus. N.H. performed optical characterizations. N.H., C.Y.H., and M.M. operated XRD measurement. N.H., R.Y., and M.S. performed TEM measurements. N.H. and A.J. analyzed the data. N.H. and D.C.C. performed the modelling of crystal growth. N.H. and A.J. wrote the manuscript. All authors discussed the results and commented on the manuscript.

Competing financial interests

The authors declare no competing financial interest.

Data Availability Statement

The data that support the findings of this study are available from the corresponding author upon reasonable request.

Corresponding Author

*E-mail: ajavey@berkeley.edu

TOC Graphic

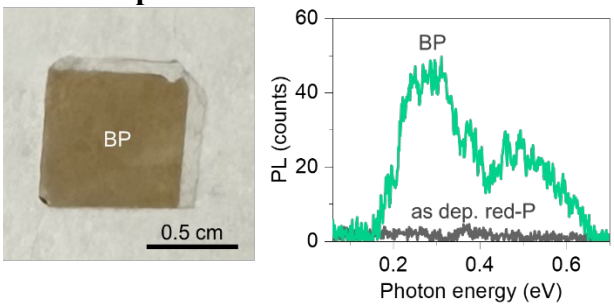
BP
0.5 cm
60
40
20
0
PL (counts)
BP
as dep. red-P
0.2
0.4
0.6
Photon energy (eV)